Nanomechanical analysis of cells from cancer patients

SARAH E. CROSS[1,2†], YU-SHENG JIN[3†], JIANYU RAO[3*†] AND JAMES K. GIMZEWSKI[1,2*†]

[1]Department of Chemistry and Biochemistry, University of California, Los Angeles, California 90095, USA
[2]California NanoSystems Institute, University of California, Los Angeles, California 90095, USA
[3]Department of Pathology and Laboratory Medicine, University of California, Los Angeles, California 90095, USA
[†]These authors contributed equally to this work.
*e-mail: gim@chem.ucla.edu; JRao@mednet.ucla.edu

Published online: 2 December 2007; doi:10.1038/nnano.2007.388

Change in cell stiffness is a new characteristic of cancer cells that affects the way they spread[1,2]. Despite several studies on architectural changes in cultured cell lines[1,3], no *ex vivo* mechanical analyses of cancer cells obtained from patients have been reported. Using atomic force microscopy, we report the stiffness of live metastatic cancer cells taken from the body (pleural) fluids of patients with suspected lung, breast and pancreas cancer. Within the same sample, we find that the cell stiffness of metastatic cancer cells is more than 70% softer, with a standard deviation over five times narrower, than the benign cells that line the body cavity. Different cancer types were found to display a common stiffness. Our work shows that mechanical analysis can distinguish cancerous cells from normal ones even when they show similar shapes. These results show that nanomechanical analysis correlates well with immunohistochemical testing currently used for detecting cancer.

Recent progress in the study of cancer cell motility and invasion has generated a greater understanding of the mechanical properties involved in malignant transformation. In particular, the dynamic reorganization of the cytoskeleton has become a specific point of interest regarding changes in cell morphology, motility, adhesion and invasion[4,5]. Techniques for measuring cell adhesion and motility have been established in the laboratory for *in vitro* analysis of cellular phenotypic events associated with tumour cells. Current cytoskeleton analysis techniques include biochemical purifications, gene expression and polymerization assays, immunofluorescent labelling, and time-lapse and electron microscopies[6,7]. Recently, a change in the physical properties, in particular cell elasticity, of tissue cells has been recognized as an indication of disease[2,8,9] and has emerged as a marker for cellular phenotypic events associated with cell adhesion and cytoskeletal organization[2,10–12]. In particular, several studies have shown a reduction in stiffness with increasing metastatic efficiency in human cancer cell lines using several different *in vitro* biomechanical assays (see, for example, refs 13–15).

In this letter we report on the associated cell stiffness (elasticity) of pathologically defined human metastatic cancer cells and benign reactive mesothelial cells in human body (pleural) fluid samples (as approved by the Institutional Review Board; Table 1) using atomic force microscopy (AFM)[16]. AFM has been used to probe a number of properties inherent to microbial cells, mammalian cells and biomolecules[10,13–15,17–22], including analysis of cellular mechanical strain and elasticity, due to the precise application of low forces to cells with minimal disruption[18,19]. Although AFM has previously been used to probe cellular mechanics under physiological conditions[13–15,21,23,24], it has not been used for cancer cell analysis in a clinical setting, which is the purpose of this letter.

Analyses of body fluid samples, rather than primary tumour samples, were chosen here, because tumour cells in body fluid are all metastatic in nature and thus provide a clonal population of metastatic cells for analysis. Additionally, the co-existence of both benign and metastatic cells in a single specimen provides a native internal control. Body cavities, including pleural, pericardial and peritoneal cavities, are covered by serous membranes consisting of a single row of flat mesothelial cells on the surface and an underlying submesothelial layer, which cover a very large surface area in close contact with every major organ of the body. Because of their continuity with the lymphatic system, these cavities are commonly the seat of metastasis. Metastatic malignant effusions constitute an unequivocal sign of widespread cancer. Current cancer cell detection relies on qualitative morphological analyses of shape change resulting from biochemical alterations, such as cytoskeletal remodelling[25]. However, morphological analysis of cells recovered from an effusion is often difficult to diagnose because of the notorious reactivity of mesothelial cells in mimicking metastatic cancer cells morphologically, featuring enlarged nuclei, increased nuclear and cytoplasmic ratios, among other cytomorphological features.

We measured the nanomechanical properties associated with the observed shape changes inherent to metastatic adenocarcinoma cells and benign mesothelial cells in pleural effusions obtained from body cavity fluid samples collected from patients with suspected metastatic adenocarcinoma, using standard protocols (see Methods). Samples were centrifuged, and cell pellets were resuspended in culture medium for 12 h, based on time-culture experiments to establish the optimum incubation time for cell-substrate adherence for mechanical analysis while minimizing artifacts resulting from *in vitro* culture. The 12 h incubation also allowed the differentiation of benign and malignant cells based on their *ex vivo* growth and morphological characteristics (that is, 'tumour' cells display anchorage-independent growth patterns, such as rounding of cells, whereas 'normal' mesothelial cells show a large, flat morphology; Fig. 1), so that AFM analysis could be performed separately on these two cell populations. These analyses were later confirmed by

Table 1 Patient characteristics and cytological diagnosis versus mechanical measurements (Young's modulus, *E*).

Case no.	Age/sex	Clinical history	Cytological diagnosis of pleural fluid*	Stiffness (kPa): 'Tumour'	Stiffness (kPa): 'Normal'
1	52/Female	Non-small cell carcinoma of the lung	Positive for metastatic malignant cells	0.56 ± 0.09	2.10 ± 0.79
2	60/Female	Non-small cell carcinoma of the lung	Positive for metastatic malignant cells	0.52 ± 0.12	2.05 ± 0.87
3	49/Female	Breast ductal adenocarcinoma	Positive for metastatic malignant cells	0.50 ± 0.08	1.93 ± 0.50
4	85/Male	Pancreatic adenocarcinoma	Positive for metastatic malignant cells	0.54 ± 0.08	0.54 ± 0.12
5	40/Male	Liver cirrhosis	Negative for malignant cells	–	1.86 ± 0.50
6	47/Male	Fever and hepatic failure	Negative for malignant cells	–	1.75 ± 0.61
7	92/Female	Anasarca peripheral oedema	Negative for malignant cells	–	2.09 ± 0.98

*Cytomorphological diagnosis was made based on morphological analysis combined with immunohistochemical analysis (see Supplementary Information). Stiffness values (*E*) represent mean ± s.d.

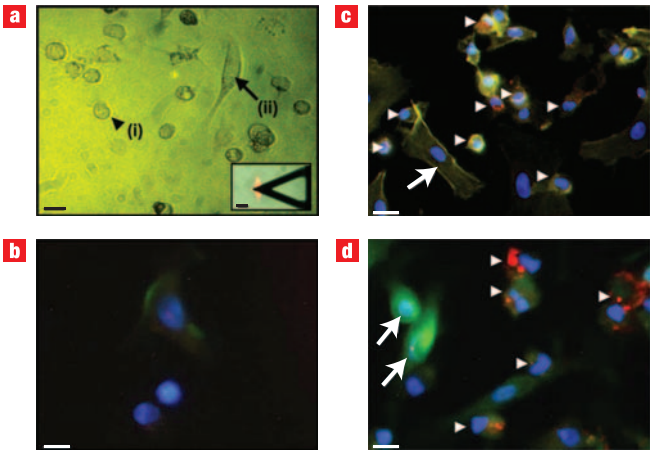

Figure 1 Optical and fluorescence images of a cytological sample. a, Optical image demonstrating the round, balled morphology of visually assigned tumour cells (i) and the large, flat morphology of presumed benign mesothelial (normal) cells (ii). The inset shows alignment of an AFM tip over the central (nuclear) region of a cell. Scale bar = 50 μm. **b**–**d**, Immunofluorescence analysis of a clinical pleural effusion displaying two cell populations (as shown in **a**): fluorescence image of the negative control (omitting primary antibodies for Ber-EP4 and Calretinin) (**b**); corresponding positive immunofluorescence triple labelling assay for DNA (blue), F-actin (green) and Ber-EP4 (red) (**c**) and for DNA, Ber-EP4 and Calretinin (DNA = blue, Ber-EP4 = red, Calretinin = green) (**d**). Arrowheads = tumour, arrow = mesothelial cells. Scale bars (main panels **a**–**d**) = 10 μm.

immunofluorescence analysis using biomarkers specific for metastatic cancer and mesothelial cells. Immunofluorescence analysis was performed independently, although on the same population of cells from the same pleural effusion sample, to confirm that cells subjected to AFM analysis based on growth characteristics indeed represented either tumour or mesothelial cells. For each sample, eight probable mesothelial ('normal') cells and eight probable malignant ('tumour') cells (except in the negative cases where only benign cells were present) were selected from their culture dish for *ex vivo* AFM analysis, which was conducted in an alternate fashion to ensure similar conditions were applied for both populations, without prior knowledge of the cytomorphological analysis. Cytomorphological (with immunohistochemical confirmatory analysis), AFM and immunofluorescence analyses were performed independently. Cytomorphological analysis was performed on its own population of cells, but the immunofluorescence and AFM analyses were made on the same population of cells; however, all of the cell populations were obtained from the same pleural effusion. Mechanical measurements were obtained at 37 °C at a rate of 1 Hz (see Methods). Force–displacement curves were recorded on each cell to determine the relative cell stiffness (Young's modulus, *E*) of individual cells, yielding values of *E* for each cell type per clinical specimen (Table 1).

To confirm the selected cell populations actually represent tumour and mesothelial cells, immunofluorescence triple labelling assays of the samples were performed (see Methods; Fig. 1b–d). Labelling for DNA/Ber-EP4/F-actin (Fig. 1c) and DNA/Ber-EP4/Calretinin (Fig. 1d) both showed staining of the small, round cells for Ber-EP4 (red), a marker for metastatic adenocarcinoma cells, thus confirming that the round, balled cells (shown optically in Fig. 1a) were indeed metastatic adenocarcinoma cells. Moreover, the large, flat cells were positive for Calretinin staining (Fig. 1d), indicative of normal mesothelial cells and consistent with the optical morphology (Fig. 1a). Immunofluorescence analysis showed that the small round cells were not apoptotic, dead or mitotic, as they have intact DNA (Fig. 1b–d, blue fluorescence).

Cell elasticity measurements (Young's modulus, *E*) taken on cytological samples collected from patients with suspected metastatic adenocarcinoma are shown in Fig. 2. Data collected from seven different clinical samples (positive for metastatic tumour, $n = 40$; negative for metastatic tumour, $n = 48$) yielded average *E* values (mean ± s.d.) for all tumour and benign mesothelial cells of 0.53 ± 0.10 kPa and 1.97 ± 0.70 kPa, respectively (Fig. 2b,c; $P = 8.72 \times 10^{-22}$). A two-sample independent *t*-test conducted on the tumour and mesothelial cell populations showed that the population means were significantly different from each other at the 95% confidence level ($P = 8.72 \times 10^{-22}$). In particular, tumour cell elasticity measurements from a single clinical sample were found to have an average cell stiffness (mean ± s.d.) of 0.56 ± 0.09 kPa (Fig. 2e); however, the average cell stiffness for the morphologically determined benign mesothelial cells in the sample expressed a significantly increased average cellular elasticity (mean ± s.d.), with a value of 2.10 ± 0.79 kPa (Fig. 2f; $P = 7.77 \times 10^{-5}$). Interestingly, the tumour and benign mesothelial cells exhibited significantly different trends; elasticity measurements for the metastatic cancer cells and the benign mesothelial cells were best fit by gaussian (normal) and log-normal fits, respectively. Tumour cells displayed a narrow, spiked peak with little spread, whereas benign mesothelial cells displayed a broad peak. Similarly, elasticity measurements collected on a single negative pleural fluid sample yielded an average cell stiffness (mean ± s.d.) of 2.09 ± 0.98 kPa (Fig. 2g; $n = 8$). The data clearly show that the cell stiffness of metastatic cancer cells is $\sim 73 \pm 11\%$ less stiff than the benign mesothelial cells in the same sample and when compared to samples collected from other patients.

Figure 2h,i shows gaussian fits of Young's modulus data collected on an individual clinical sample (Table 1, Case 4) containing only one population of cells, which were difficult to determine as either benign mesothelial cells or metastatic malignant cells, based on cytomorphology. However, following

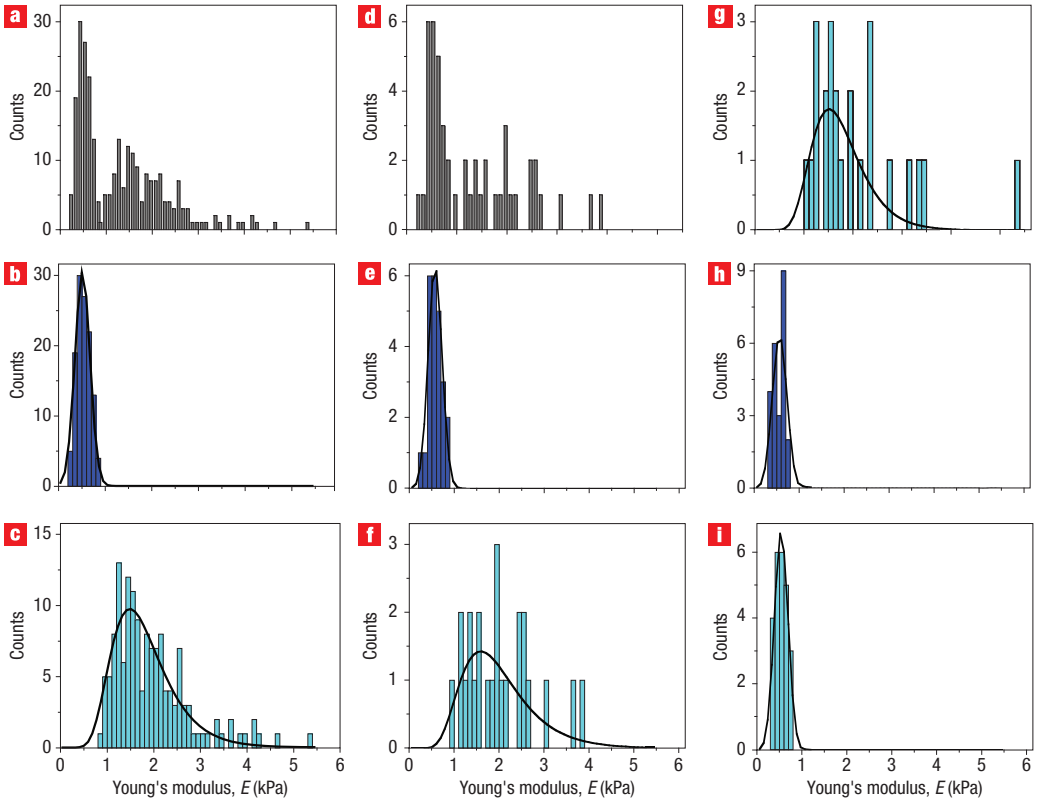

Figure 2 Histograms of the associated Young's modulus *E* for cytological samples collected from patients with suspected metastatic cancer. a, Histogram of *E* for all data collected from seven different clinical samples (tumour, $n = 40$; normal, $n = 48$). **b**, Gaussian fit for all tumour data from the seven samples. **c**, Log-normal fit for all normal data from the samples. **d**–**f**, Data from a single clinical sample: values of *E* for all cells (**d**), gaussian fit of tumour cells (**e**), and log-normal fit of normal cells (**f**) for this sample. **g**, Histogram of *E* with log-normal fit for a single negative sample. **h**,**i**, Gaussian fits of visually diagnosed metastatic (tumour, **h**) and mesothelial (normal, **i**) cells in an individual clinical sample (Table 1, Case 4).

ex vivo culture there still appeared to be two populations of cells, one cell type that was larger and more flat, suggestive of benign mesothelial cells, and the other type, which was more round and balled up, suggestive of tumour cells. Despite the difference of morphology in *ex vivo* culture, nanomechanical analysis concluded that these were all tumour cells. Average values (mean $\pm$ s.d.) for both the tumour and morphologically classified benign mesothelial cells were 0.54 ± 0.08 kPa and 0.54 ± 0.12 kPa, respectively (Fig. 2 h,i; $n = 8$). These population means were not statistically different, and indicated the presence of a single population of malignant cells. Subsequent immunohistochemical staining (IHC) with a battery of markers including Calretinin, B72.3 and Ber-EP4 (see Supplementary Information) confirmed that the sample contained predominantly one cell population, which was indeed malignant based on IHC findings (negative for Calretinin and positive for Ber-EP4 and B72.3). Additionally, this particular case demonstrates no correlation between *ex vivo* cultured cell morphology and expected measured stiffness. This lack of correlation suggests that it is unlikely that the *ex vivo* cultured morphological differences influence measured elasticity.

For each individual patient effusion a new cantilever was used, to avoid any contribution of possible artifacts. The similarity in the data from patient to patient and cell to cell is strongly suggestive of a parallel between patient effusions and cell type. To further confirm that the measured differences between tumour and benign cells were not an artifact of *ex vitro* culturing, we used a modified cytocentrifugation procedure without *ex vivo* culturing, which yielded morphologically indistinguishable cell types. The resulting Young's modulus values for tumour and benign mesothelial cells were analogous to those obtained using the 12 h *ex vivo* culture method (see Supplementary Information for more details). This correlation of cell stiffness for the tumour and normal cells in the pleural effusions experimentally demonstrates that the mechanical analysis is representative of cell type, even when considering different preparation methods and the use of different substrates.

The need for biomarkers for cancer detection and analysis is critical due to the complexity of the disease. This study shows important implications for the combined use of imaging analysis with nanomechanical measurements as a novel biomarker for evaluating and sensing changes in tumour cells, and which is easily translated into clinical settings. Our results suggest that a shift in biologically driven biomechanical properties towards a decrease in cell stiffness correlates with an increase in metastatic potential. Under analogous conditions, cell stiffness of metastatic cancer cells is $>70\%$ lower than normal reactive mesothelial cells in the same sample, when compared to other pleural effusions, or even for patients with different clinical histories (Table 1). This finding is consistent with previous studies, which found a decrease in stiffness of human cancer cell lines with increasing metastatic efficiency using different single-cell *in vitro* biomechanical assays[13–15]. Despite morphological overlap between tumour and normal cell types, which often poses a significant problem for cytomorphological and immunohistochemical

diagnosis of malignant cells, mechanical analysis provides the ability to distinguish cancer cells. These findings clearly demonstrate the ability of nanomechanical-based functional analysis to detect metastatic tumour cells in body fluid. Likewise, the distribution of measured cell stiffness for tumour cells is over five times narrower than the corresponding distribution for benign mesothelial cells. We found that tumour cell stiffness fits with a normal distribution, whereas the measured benign mesothelial cell stiffness values better fit a log-normal distribution. The finding that no quantitative overlap was observed in the measured cell elasticity values collected for the metastatic tumour and reactive mesothelial cells is of major diagnostic significance. Cancer is extremely biochemically diverse, yet mechanically a common modulus for each cell type is exhibited even for different tumour types and patient effusions (Table 1). The correlation of cytomechanical measurements with immunohistochemical analysis suggests that nanomechanical measurements of cancer cells has potential for the detection of cancer and may aid in personalized selection of medication and drug screening, especially in body cavity effusions where accurate diagnosis based solely on morphology has to date been challenging.

METHODS

CYTOLOGICAL SAMPLE COLLECTION

The body cavity fluid samples were collected and processed using a standard protocol in cytology labs for conventional cytological analysis including Papanicolaou stain, Gimsa stain and cellblock preparation. An aliquot of the remaining sample (10 ml) was centrifuged at 500*g* for 10 min. Cell pellets were resuspended with MEM-F12 culture medium and incubated for 12 h at 37 °C in 5% CO_2 and 95% air. The culture medium was changed immediately before AFM analysis to wash off any dead and untouched cells.

NANOMECHANICAL MEASUREMENTS WITH AFM

All studies were conducted using a Nanoscope IV Bioscope (Veeco Digital Instruments) with a combined inverted optical microscope (Nikon eclipse TE200). This combination permitted lateral positioning of the AFM tip over the nuclear region of the cell with micrometre precision (Fig. 1a, inset). The scan size for all measurements was set to 0 nm to maintain a constant position over the cell, and using the AFM software the tip was brought into contact with the central region of the cell[26]. Mechanical measurements were collected at 37 °C using sharpened silicon nitride cantilevers with experimentally determined[27] spring constants of 0.02 N m^{-1} and a tip radius of $<$20 nm.

Force–displacement curves were recorded at 1 Hz for determination of Young's modulus *E*. *E* was calculated by converting the force curves into force–indentation curves[28] and fitting with the Hertz model, which describes the indentation of an elastic sample using a stiff conical indenter, as described elsewhere[10,29]. The half opening angle of the AFM tip was 36° and the Poisson ratio of the cell was taken to be 0.5, as is typical for soft biological materials[28]. To prevent damage to the cell surface and to reduce any possible substrate-induced effects, measurements were analysed in force ranges resulting in shallow indentations of the cell ($<$400 nm)[30].

IMMUNOFLUORESCENCE TRIPLE LABELLING

Two types of triple labelling assays were performed, one was DNA/F-actin/Ber-EP4 and the other DNA/Calretinin/Ber-EP4. For both experiments, cells were fixed first with 3.7% formaldehyde for 30 min at room temperature and then washed with 1× PBS three times, then incubated with 1% BSA in PBS pH 7.4 for 30 min. For DNA/F-actin/Ber-EP4 labelling, cells were first incubated with mouse anti-human Ber-EP4 (DAKO) at 1:300 dilution for 1 h, followed by Cy3-conjugated AffiniPure goat anti-mouse IgG(H + L) (Jackson ImmunoResearch Lab) at 1:200 dilution for 30 min, then with BODIPY FL phallacidin F-actin (Molecular Probes) at 1:40 dilution for 30 min. Finally, cells were incubated with 1:10,000 DAPI for 5 min. For DNA/Calretinin/Ber-EP4 labelling, cells were first incubated with mouse anti-human Ber-EP4 (DAKO) at 1:300 dilution for 1 h, followed by Cy3-conjugated AffiniPure goat anti-mouse IgG(H + L) (Jackson ImmunoResearch Lab) at 1:200 dilution for 30 min. Cells were then further incubated with 1:600 diluted rabbit anti-human Calretinin antibody (Zymed) for 1 h then with FITC-conjugated AffiniPure goat anti-rabbit IgG(H + L) (Jackson ImmunoResearch Lab) at 1:50 dilution for 30 min, followed by 1:10,000 DAPI for 5 min. All incubations were performed at room temperature and there were three PBS washing steps in between. Cells were covered with mounting medium for fluorescence microscopic examination. Images were taken using an Olympus BX-40 microscope with a ×40 objective.

STATISTICAL ANALYSIS

Data were expressed as mean ± s.d., and the statistical significance of differences in mean values was assessed using a two-sample independent Student's *t*-test at the 95% confidence level. Differences among means are reported using exact *P* values.

Received 9 September 2007; accepted 19 October 2007;
published 2 December 2007.

References

1. Bhadriraju, K. & Hansen, L. K. Extracellular matrix- and cytoskeleton-dependent changes in cell shape and stiffness. *Exp. Cell Res.* **278,** 92–100 (2002).
2. Discher, D., Janmey, P. & Wang, Y. Tissue cells feel and respond to the stiffness of their substrate. *Science* **310,** 1139–1143 (2005).
3. Radmacher, M. Measuring the elastic properties of biological samples with the AFM. *IEEE Eng. Med. Biol. Mag.* **16,** 47–57 (1997).
4. Yamazaki, D., Kurisu, S. & Takenawa, T. Regulation of cancer cell motility through actin reorganization. *Cancer Sci.* **96,** 379–386 (2005).
5. Rao, J. & Li, N. Microfilament actin remodeling as a potential target for cancer drug development. *Curr. Cancer Drug Targ.* **4,** 267–283 (2004).
6. Motherby, H. *et al.* Pleural carcinosis confirmed by adjuvant cytological methods: A case report. *Diag. Cytopathol.* **19,** 370–374 (1998).
7. Osterheld, M., Liette, C. & Anca, M. M. D. Image cytometry: an aid for cytological diagnosis of pleural effusions. *Diag. Cytopathol.* **32,** 173–176 (2005).
8. McKnight, A. L. *et al.* MR elastography of breast cancer: preliminary results. *AJR Am. J. Roentgenol.* **178,** 1411–1417 (2002).
9. Bercoff, J. *et al. In vivo* breast tumor detection using transient elastography. *Ultrasound Med. Biol.* **29,** 1387–1396 (2003).
10. Rotsch, C. & Radmacher, M. Drug-induced changes of cytoskeletal structure and mechanics in fibroblasts: an atomic force microscopy study. *Biophys. J.* **78,** 520–535 (2000).
11. Lee, J., Ishihara, A. & Jacobson, K. How do cells move along surfaces? *Trends Cell Biol.* **3,** 366–370 (1993).
12. Stossel, T. P. On the crawling of animal cells. *Science* **260,** 1086–1094 (1993).
13. Suresh, S. *et al.* Connections between single-cell biomechanics and human disease states: gastrointestinal cancer and malaria. *Acta Biomaterialia* **1,** 15–30 (2005).
14. Guck, J. *et al.* Optical deformability as an inherent cell marker for testing malignant transformation and metastatic competence. *Biophys J.* **88,** 3689–3698 (2005).
15. Suresh, S. Biomechanics and biophysics of cancer cell. *Acta Biomaterialia* **3,** 413–438 (2007).
16. Binnig, G., Quate, C. & Gerber, C. Atomic force microscope. *Phys. Rev. Lett.* **56,** 930–933 (1986).
17. Rotsch, C., Braet, F., Wisse, E. & Radmacher, M. AFM imaging and elasticity measurements on living rat liver macrophages. *Cell Biol. Int.* **21,** 685–696 (1997).
18. Charras, G. T. & Horton, M. A. Single cell mechanotransduction and its modulation analyzed by atomic force microscopy indentation. *Biophys. J.* **82,** 2970–2981 (2002).
19. Dufrene, Y. F. Atomic force microscopy, a powerful tool in microbiology. *J. Bacteriol.* **184,** 5205–5213 (2002).
20. Pelling, A. E., Li, Y., Shi, W. & Gimzewski, J. K. Nanoscale visualization and characterization of *Myxococcus xanthus* cells with atomic force microscopy. *Proc. Natl Acad. Sci. USA* **102,** 6484–6489 (2005).
21. Pelling, A. E., Sehati, S., Gralla, E. B., Valentine, J. S. & Gimzewski, J. K. Local nanomechanical motion of the cell wall of *Saccharomyces cerevisiae*. *Science* **305,** 1147–1150 (2004).
22. Rief, M., Gautel, M., Oesterhelt, F., Fernandez, J. M. & Gaub, H. E. Reversible unfolding of individual titin immunoglobulin domains by AFM. *Science* **276,** 1109–1112 (1997).
23. Kasas, S., Gotzos, V. & Celio, M. R. Observation of living cells using the atomic force microscope. *Biophys. J.* **64,** 539–544 (1993).
24. Hansma, P. K. *et al.* Tapping mode atomic force microscopy in liquids. *Appl. Phys. Lett.* **64,** 1738–1740 (1994).
25. Salgia, R. *et al.* Expression of the focal adhesion protein paxillin in lung cancer and its relation to cell motility. *Oncogene* **18,** 67–77 (1999).
26. Wu, H. W., Kuhn, T. & Moy, V. T. Mechanical properties of 1929 cells measured by atomic force microscopy: effects of anticytoskeletal drugs and membrane crosslinking. *Scanning* **20,** 389–397 (1998).
27. Levy, R. & Maaloum, M. Measuring the spring constant of atomic force microscope cantilevers: thermal fluctuations and other methods. *Nanotechnology* **13,** 33–37 (2002).
28. Touhami, A., Nysten, B. & Dufrene, Y. F. Nanoscale mapping of the elasticity of microbial cells by atomic force microscopy. *Langmuir* **19,** 4539–4543 (2003).
29. Matzke, R., Jacobson, K. & Radmacher, M. Direct, high-resolution measurement of furrow stiffening during division of adherent cells. *Nature Cell Biol.* **3,** 607–610 (2001).
30. Stolz, M. *et al.* Dynamic elastic modulus of porcine articular cartilage determined at two different levels of tissue organization by indentation-type atomic force microscopy. *Biophys. J.* **86,** 3269–3283 (2004).

Acknowledgements

S.E.C. and J.K.G. acknowledge partial support from National Institutes of Health research grant no. 5 R21 GM074509 and from the Institute for Cell Mimetic Space Exploration, a National Aeronautics and Space Administration University Research Engineering Technology Institute. J.R. and Y.J. acknowledge partial support from National Institutes of Health research grant no. U01CA96116 and Alper grant, Johnsson Comprehensive Cancer Center.

Correspondence and requests for materials should be addressed to J.K.G. and J.R.

Supplementary information accompanies this paper on www.nature.com/naturenanotechnology.

Author contributions

S.E.C., Y.J., J.R. and J.K.G. contributed equally to this work.